Received: 19 March 2024 | Accepted: 23 August 2024

DOI: 10.1002/ajb2.16438

RESEARCH ARTICLE

Botany

Phosphoproteomic analysis of distylous *Turnera subulata* identifies pathways related to endoreduplication that correlate with reciprocal herkogamy

Paige M. Henning[1] | **Benjamin B. Minkoff**[1] | **Michael R. Sussman**[1,2]

[1]Center for Genomic Science Innovation, University of Wisconsin–Madison, 425 Henry Mall, Madison, Wisconsin 53706, USA

[2]Department of Biochemistry, University of Wisconsin–Madison, 433 Babcock Drive, Madison, Wisconsin 53706, USA

Correspondence

Paige M. Henning, Center for Genomic Science Innovation, University of Wisconsin–Madison, 425 Henry Mall, Madison, Wisconsin 53706, USA.
Email: phenning3@wisc.edu

Abstract

Premise: A multi-omic approach was used to explore proteins and networks hypothetically important for establishing filament dimorphisms in heterostylous *Turnera subulata* (Sm.) as an exploratory method to identify genes for future empirical research.

Methods: Mass spectrometry (MS) was used to identify differentially expressed proteins and differentially phosphorylated peptides in the developing filaments between the L- and S-morphs. RNAseq was used to generate a co-expression network of the developing filaments, MS data were mapped to the co-expression network to identify hypothetical relationships between the *S*-gene responsible for filament dimorphisms and differentially expressed proteins.

Results: Mapping all MS identified proteins to a co-expression network of the S-morph's developing filaments identified several clusters containing SPH1 and other differentially expressed or phosphorylated proteins. Co-expression analysis clustered CDKG2, a protein that induces endoreduplication, and SPH1—suggesting a shared biological function. MS analysis suggests that the protein is present and phosphorylated only in the S-morph, and thus active only in the S-morph. A series of CDKG2 regulators, including ATM1, and cell cycle regulators also correlated with the presence of reciprocal herkogamy, supporting our interest in the protein.

Conclusions: This work has built a foundation for future empirical work, specifically supporting the role of CDKG2 and ATM1 in promoting filament elongation in response to SPH1 perception.

KEYWORDS

CDKG2, distyly, endoreduplication, herkogamy, heterostyly, reproduction, S-protein homolog

Angiosperms are considered the most successful plant lineage, accounting for ~80% of known plant life (Benton et al., 2022; Sauquet et al., 2022). This success is largely attributed to the evolution of the flower and fruit (Benton et al., 2022). Since the evolution of the flower, a vast number of reproductive strategies have evolved within Angiospermae to promote outcrossing and prevent inbreeding depression due to selfing either through physical or biochemical means (Franklin-Tong, 2008; Cardoso et al., 2018). Herkogamy, the physical separation of the stigma and anther (Figure 1A), is an example of a modification that promotes outcrossing by decreasing the probability of self-pollen landing on self-stigma (Luo and Widmer, 2013; Jiang et al., 2018).

Reciprocal herkogamy is a unique dimorphism exhibited by distylous species. Distylous species have two floral morphs: the L-morph, which exhibits typical herkogamy, and the S-morph, which exhibits "reverse

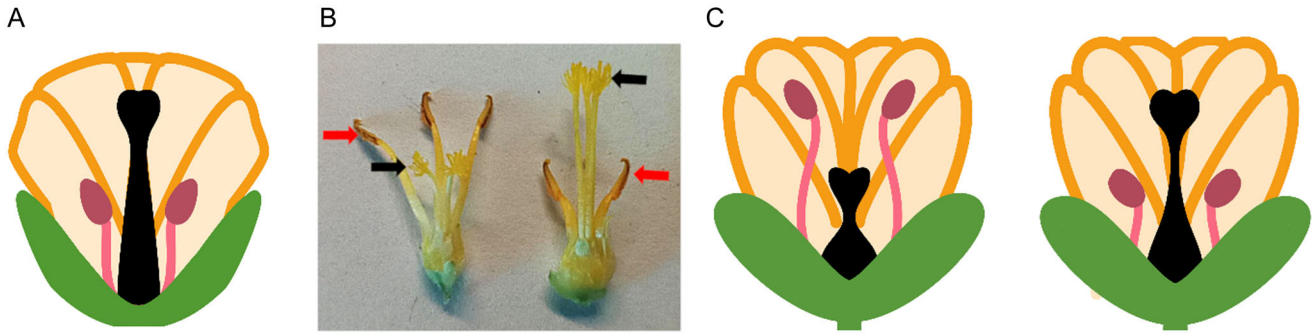

FIGURE 1 Reciprocal herkogamy in distylous *Turnera subulata*. (A) Diagram of typical herkogamous flower. (B) Photograph of the S-morphs (left) and L-morphs (right) of distylous *T. subulata*, which exhibits reciprocal herkogamy, as diagrammed in (C). Petals are outlined in orange, pistils are black, stamens are pink/magenta, sepal and stem are green (A, B) (differences in sepal and petal shape are arbitrary artifacts of the artist's drawing ability). Red arrows indicate top of anthers; black arrows denote top of stigma. Additional photos of the dissected flowers can be found in Appendix S1: Figure S1A–D.

herkogamy" in which the stigma is placed lower in the flower and the anthers higher (Figure 1B, C; Appendix S1: Figure S1; Darwin, 1877; Barrett, 2019). In conjunction with the evolution of self-incompatibility in distylous species, reverse herkogamy likely evolved to further increase outcrossing and reproductive success as it promotes disassortative mating due to the nature of pollen deposition on the pollinators (Karron et al., 2021). For example, pollen from S-morph individuals is deposited on the lower thorax and abdomen of the pollinator, where it is more likely to contact the stigma of an L-morph individual.

In addition to its unique herkogamy, distyly is an exceptional case of convergent evolution. It is found in ≥28 families and ≥199 genera, all of which display reciprocal herkogamy and some degree of self-incompatibility (Naiki, 2012; Barrett, 2019). Convergence of the system goes beyond morphology, seemingly occurring at the biochemical, transcriptional, and genomic levels (Henning et al., 2020; Potente et al., 2022). The most strongly supported example of convergence beyond morphology is the genetic basis of distyly, which cumulative research suggests is always a hemizygous supergene, present only in the S-morph's genome (Cocker et al., 2018; Shore et al., 2019; Gutiérrez-Valencia et al., 2022; Fawcett et al., 2023; Yang et al., 2023; Zhao et al., 2023). In *Turnera* (Passifloraceae), this supergene is composed of three *S*-genes, *BAHD*, *SPH1*, and *YUC6*, making it one of the simplest known *S*-loci (Shore et al., 2019). While the roles of *BAHD* (Matzke et al., 2020, 2021) and *YUC6* (Henning et al., 2022) have been explored, little is known of *SPH1* beyond its predicted role of encouraging filament elongation in the S-morph (Shore et al., 2019).

In addition to genomic convergences, brassinosteroids' inactivation represses style elongation in the S-morph and establishes the S-morph's female mating type in both *Primula* and *Turnera*, though by different enzymes, suggesting convergence at the biochemical level (Huu et al., 2016, 2021; Matzke et al., 2020, 2021). It's further hypothesized that PHYTOCHROME-INTERACTING FACTOR (PIF) pathways help establish style length dimorphisms, as PIF pathways regulate general elongation (de Lucas and Prat, 2014). The PIF pathway hypothesis has been supported in several genera using bioinformatics and based on the hypothetical roles of recently discovered *S*-genes (Henning et al., 2020; Yang et al., 2023; Zhao et al., 2023), suggesting convergence at the transcriptional level.

Potential convergence of male-associated traits has not been explored, likely due to a lack of information regarding male-related traits. Expansion of -omic related resources is critical for the identification of potential convergences of male associated traits.

Anther height dimorphisms have been explored only in *Primula*, in which a MADS-BOX gene, GLO^{T}, coordinates cell proliferation of the corolla below the stamen in the S-morph. In some species, GLO^{T} also promotes cell elongation (Huu et al., 2020). In *Turnera*, anther height dimorphisms are a result of increased filament elongation in the S-morph, which is likely promoted by an *S*-gene *S-protein homolog 1* (*SPH1*), a cysteine-rich peptide whose perception and downstream signaling likely result in filament elongation (Shore et al., 2019).

The function of the *SPH* family is essentially unknown. The family was initially identified in self-incompatible *Papaver rhoeas*, which possesses a gametophytic self-incompatibility system; allelic peptides of one family member, PrsS (homolog of *Arabidopsis thaliana SPH2*), are secreted from the stigma to establish female mating type via interactions with its pollen tube-expressed receptor PrpS (Franklin-Tong et al., 1995; Walker et al., 1996; de Graaf et al., 2012).

The genes and mechanistic pathways underlying the morphology and self-incompatibility of the L-morph are not well known. Using a multi-omic approach, we have identified a series of proteins and pathways that may be involved in distylous *Turnera subulata* (Sm.) filament elongation. Microscopy results suggest that cell elongation is important for establishing filament elongation in the S-morph, while mass spectrometry (MS) results suggest that endoreduplication is important for establishing dimorphisms.

Our cumulative data lead us to hypothesize that CDKG2 and ATM1 are unlinked modifier genes involved in promotion of filament elongation in the S-morph of *Turnera*. Thus, this work posits the first hypotheses regarding the evolution of herkogamy in the L-morph, is the first multi-omic analysis of any heterostylous species to date, and will be a valuable resource for further studies in *Turnera* and future efforts toward understanding the convergent nature of distyly.

MATERIALS AND METHODS

Morphology

The pistils and filaments from five flowers (total 15 pistils and 25 filaments) per developmental stage were dissected and measured. The ratio of pistil to filament length across time was determined by taking the average of all filaments and all pistils of an individual flower. Stigma-anther separation was determined by measuring the distance from the top or bottom of the anther to the top of the stigma for seven open flowers. Filaments from three open flowers were dissected using a razor, photographed using a light microscope, and the length of 50 epidermal cells per filament per flower (total 150) were measured. All measurements were determined using ImageJ2 (Rueden et al., 2017). Comparisons of mean cell length significance were determined using Student's *t*-test.

Protein isolation, digestion, and phosphopeptide enrichment

The filaments of fifteen 12–14 mm buds (with a focus on 13 mm—the developmental point when SPH1 peaks in expression) were collected from the L- and S-morph of *T. subulata* (Sm. 4x/an autotetraploid) and stored at −80°C until collection was completed. Protein was isolated following the protocol provided in Appendix S1: Method S1. Protein concentration was quantified using a BCA assay (Thermo Fisher Scientific, Madison, Wisconsin, USA, catalog no. 23225) and a Thermo Fisher Scientific Nanodrop 2000; 415 µg of protein was added to a Trypsin/Lys-C digest following the manufacture's protocol (Promega, Madison, Wisconsin, USA catalog no. V5071). After an overnight digestion, peptides were cleaned using Sep-Pak C18 cartridges and accompanying protocol (Waters, Milford, Massachusetts, USA, catalog no. WAT054955).

High-Select TiO2 Phosphopeptide Enrichment Kit and accompanying protocol (Thermo Fisher Scientific, catalog no. A32993) was used for enrichment of phosphorylated peptides. Flowthrough was retained and cleaned using Sep-Pak C18 cartridges.

Mass spectrometer—flowthrough samples

All solvents used are from Fisher Scientific unless otherwise mentioned. Samples were resuspended into 20 µL Optima-LCMS 0.1% formic acid and, with a Dionex Ultimate 3000 RSLCnano System, 2 µL of this was injected onto a PepMap RSLC C18 column (Thermo Fisher Scientific) with 2 µm bead size, 100 Å pore size, and dimensions 75 µm × 50 cm for LC/MS analysis. For LC conditions, all flow rates were 300 nL/min; solvent A was Optima-LCMS 0.1% formic acid, solvent B was Optima-LCMS 0.1% formic acid/80% acetonitrile, column was heated to 50°C, and gradient conditions were as follows: background running conditions, 2% B, 1–2 min to 5% B, 2–162 min to 37.5% B, 162–167 min to 95% B, 167–172 min consistent 95% B, 172–174 min to 2% B then flowed at 2% B until the end of the run/acquisition at 180 min. Sample was sprayed off the column at 1900 V into a Thermo Fisher Scientific Orbitrap Fusion Lumos, and all data were collected in positive mode. Data-dependent acquisition was used. MS1 spectra were acquired in profile mode in the Orbitrap mass analyzer with 120 K resolution, quadrupole isolation, a scan range of 350–1600 m/z, RF lens 30%, normalized AGC target 250%, and a max inject time of 50 ms. Monoisotopic peak filtering was set to peptide, charge state filtering 2–4, and dynamic exclusion ($n = 1$) for 10 s, and a window of ±10 ppm was set between MS1 and MS2 scans. MS2 spectra were acquired in positive mode in the ion trap with quadrupole isolation of 0.7 Da, HCD fragmentation with a collision energy of 30%, scan rate set to turbo mode, mass range set to normal, scan range mode set to auto, a custom AGC target 300%, in centroid mode, with a max inject time of 25 ms. In between MS1 scans a cycle time of 1 s was set as fixed.

Mass spectrometer—phosphopeptide-enriched samples

All solvents used are from Fisher Scientific unless otherwise mentioned. Samples were resuspended into 10 µL Optima-LCMS 0.1% formic acid and, with a Dionex Ultimate 3000 RSLCnano System, 5 µL of this was injected onto a PepMap RSLC C18 column (Thermo Fisher Scientific) with 2 µm bead size, 100 Å pore size, and dimensions 75 µm × 50 cm for LC/MS analysis. For LC conditions, all flow rates were 300 nL/min, solvent A is Optima-LCMS 0.1% formic acid, and solvent B is Optima-LCMS 0.1% formic acid/80% acetonitrile; column was heated to 50°C, and gradient conditions were as follows: background running conditions, 2% B, 1–2 min to 5% B, 2–95 min to 37.5% B, 95–105 min to 95% B, 110–110.1 min to 2% B, then flowed at 2% B until the end of the run/acquisition at 120 min. Sample was sprayed off the column at 1900 V into a Thermo Fisher Scientific Orbitrap Fusion Lumos, and all data were collected in positive mode. Data-dependent acquisition was used. MS1 spectra were acquired in profile mode in the Orbitrap mass analyzer with 120 K resolution, quadrupole isolation, a scan range of 350–1600 m/z, RF lens 30%, normalized AGC target 250%, and a max inject time of

50 ms. Monoisotopic peak filtering was set to peptide, charge state filtering 2–7, and dynamic exclusion ($n = 1$) for 10 s, and a window of ±10 ppm was set between MS1 and MS2 scans. MS2 spectra were acquired in positive mode in the ion trap with quadrupole isolation of 0.7 Da, HCD fragmentation with a collision energy of 32%, scan rate set to turbo mode, mass range set to normal, scan range mode set to auto, a custom AGC target of 300%, in centroid mode, with a max inject time of 25 ms. In between MS1 scans a cycle time of 1 s was set as fixed. The MS proteomics data have been deposited to the ProteomeXchange Consortium via the PRIDE (Perez-Riverol et al., 2022) partner repository with the data set identifier PXD049414.

Computational analysis of MS data

MS/MS files were analyzed with Proteome Discoverer version 2.4.1.15, using the workflow outlined in Appendix S1: Figure S2. Default parameters were used with the following exceptions. Precursor ion quantifier, 5. Quan. Rollup and Hypothesis testing: *t*-test (background base); Sequest HT, dynamic modifications: Phospho (S,T,Y). Peptides were aligned to the *T. subulata* (2x) genome, as this is the only genome publicly available for any species of *Turnera*. For statistical analyses, the L-morph was treated as the control because it lacks the *S*-locus.

The PhosPhAT database version 4.0 (Heazlewood et al., 2008; Durek et al., 2010) was used to identify previous published phosphorylation events for the *Arabidopsis* homologs.

RNAseq

The filaments of three 12–14 mm buds (with a focus on 13 mm buds) were collected from the S-morph of *T. subulata* (4x). Each flower of *T. subulata* contains a total of five filaments. RNA was isolated from filaments using PureLink Plant RNA Reagent following the accompanying small-scale protocol (ThermoFisher, Madison, Wisconsin, USA, catalog no. 12322012) and treated with DNase I (Invitrogen, Waltham, Massachusetts, USA catalog no. 18047019). A total of 35 replicates were produced ($n = 20$ from 3-yr-old mother plant, $n = 5$ from each of three offspring); these 35 samples were sequenced (150 bp paired end reads) and filtered by NovoGene (Sacramento, California, USA) using an Illumina NovaSeq. 6000. Raw data can be found at GenBank (Bioproject no. PRJNA1054211).

Co-expression network

All Linux programs were run using Ubuntu release 22.19, and R-scripts were executed using R version 4.3.2 (RStudio Team, 2020; R Core Team, 2023). Co-expression networks were generated using HISAT2 version 2.2.1 (Pertea et al., 2016), Samtools version 1.13 (Danecek et al., 2021), STRINGTie version 2.2.1 (Pertea et al., 2016), and R packages "WGNCA" version 1.72-1 and "flastcluster" version 1.2.3. Reads were mapped to the *T. subulata* (2x) genome (GenBank ASM2838606v3; Henning et al., 2023). Parameters, commands, and dependency versions can be found in Appendix S1, method S2. Co-expression networks were visualized using Cytoscape version 3.9.1 (Shannon, 2003). The Cytoscape STRING app version 2.0.2 (Doncheva et al., 2019) was used to identify empirically supported *Arabidopsis* networks and enriched/depleted Gene Ontology (GO) terms using a confidence score of 0.700. All networks were uploaded to NDex (Appendix S1: Table S1; Pillich et al., 2017).

Comparative genome analysis

The closest paralogs of TsSPH1 and TjSPH1 (Henning et al., 2023) were compared to the genomes of five members of Malipigales (Appendix S1: Tables S4 and S5) using command line tBLASTn and an e-value of <0.01 (Altschul et al., 1997; Schaffer et al., 2001). Identified homologs were hand annotated with the aid of the National Center for Biotechnology Information's ORF finder (https://www.ncbi.nlm.nih.gov/orffinder/). MEGA11 was used for muscle alignment and construction of maximum likelihood phylogenetic trees using the Tamura-Nei (nucleotide) and JTT (protein) models with default settings (Jones et al., 1992; Tamura and Nei, 1993; Edgar, 2004; Tamura et al., 2021). Subcellular localization was predicted using Plant-mSubP with default settings (Sahu et al., 2020). Expression data for *Salix* and *Populus* were pulled from Phytozome (Goodstein et al., 2012), data for *Manihot* from an expression atlas (Wilson et al., 2017), and *Turnera* from a previous transcriptome study (Henning et al., 2020).

RESULTS

Cell elongation helps establish filament dimorphisms in *Turnera*

To expand our understanding of herkogamy in *Turnera*, we measured filament and style length of the morphs of distylous *T. subulata* throughout development (Figure 2A–C). We found that style and filament dimorphisms are observable during the same stage that their respective *S*-genes peak in expression (Shore et al., 2019). Herkogamy is established in a linear fashion in both morphs but more rapidly in the L-morph, as determined by the best polynomial fit (L-morph = 0.2954x + 0.9497; S-morph = 0.08165x + 0.991; Figure 2C).

Given that the distance between the stigma and anther is correlated with the degree of self-incompatibility, and *Turnera* is virtually rigorously self-incompatible, we measured the distance between the top and bottom of the anther to the top of the stigma (Figure 2D). While the distance between the top of the anther and the stigma do not differ

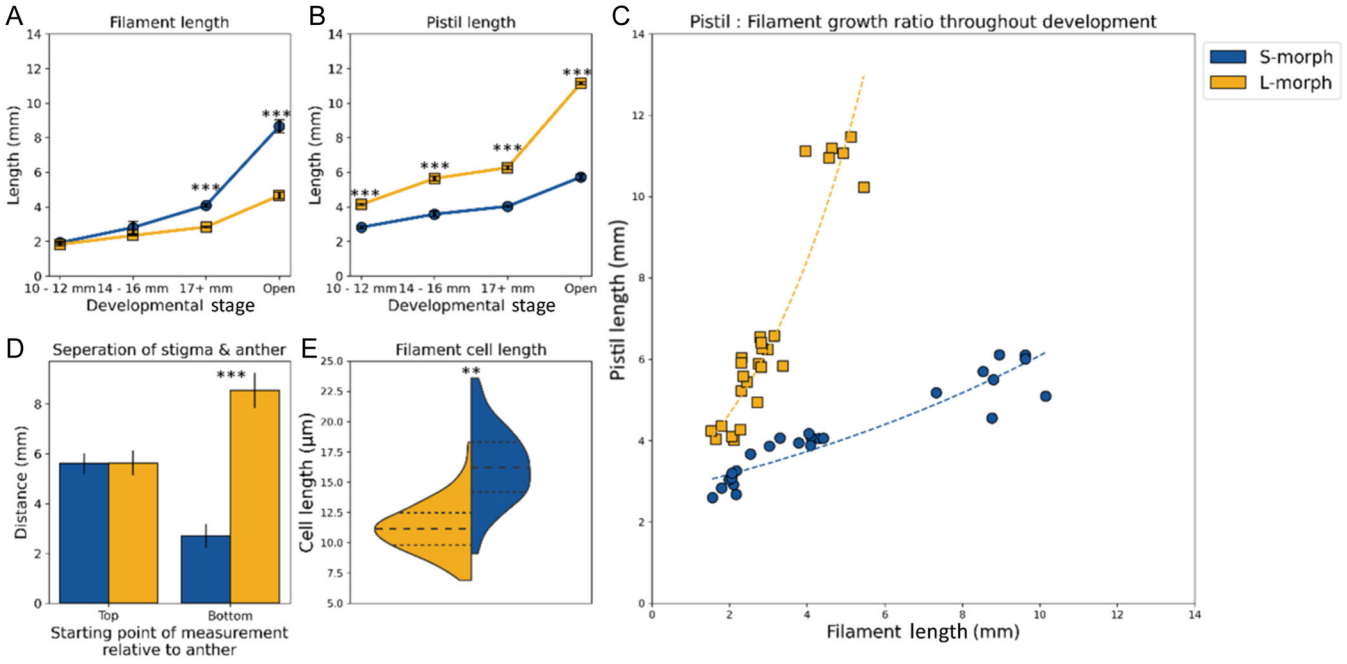

FIGURE 2 Quantification of traits associated with reciprocal herkogamy in distylous *Turnera subulata*. Average length of filaments (A) and pistils (B) throughout development. (C) Comparison of pistil to filament length throughout development, dashed line denoting line of best polynomial fit (L-morph = 0.2954x + 0.9497; S-morph 0.08165x + 0.991). (D) Distance between the anther and stigma within an open flower. (E) Length of cells of the mature filaments from the two morphs. $^{**}p < 5 \times 10^{-3}$; $^{***}p < 5 \times 10^{-5}$. Significance was calculated using Student's *t*-test; in the case of cell length, significance was calculated for the average cell length of each replicate to prevent basis due to an artificially inflated replicate number. (A–C) $n = 5$ buds = 25 filaments or 15 pistils. (D) $n = 7$. (E) $n = 3$ open flowers (50 cells/flower = total 150 cells). All error bars represent standard error.

between morphs, there is a significant difference in the distance between the anther's bottom and stigma, with the distance between the S-morph's anthers and stigma shorter than that of the L-morph.

To explore the potential role of cell elongation in the establishment of dimorphisms, we measured cell length in the filament of the open flowers of the S- and L-morphs of *T. subulata*. We found that the cells in the filaments of the S-morph of *T. subulata* are significantly longer than those in the L-morph (Figure 2E), suggesting that anther height dimorphisms are established via increased cell elongation in the S-morph.

Proteomic analysis reveals the role of cell proliferation in the establishment of filament dimorphisms

MS analysis of the *Turnera* proteome is now feasible, due to the publication of the annotated *T. subulata* (2x) genome (Henning et al., 2023). Using its associated proteome, we used MS to identify and quantify peptides from the developing filaments of the S- and L-morphs to determine if differential protein expression is correlated with filament dimorphisms. We identified 55,758 peptides corresponding to 5516 unique proteins (Appendix S1: Figure S3A, B; Appendix S2). Of these, 35 proteins were differentially expressed ($p < 0.01$), with fold change (FC) ≤ 0.05 or ≥1.5 between the two floral morphs respectively (S/L): 13 were L-morph-specific (detected in all L-morph replicates and not detected in any S-morph replicates), and 13 were S-morph-specific (Appendix S1: Table S2).

Among the L-morph-specific proteins, we were primarily interested in Tsubulata_005706, a hypothetical plant subtilase. Subtilases belong to a family of serine peptidases involved in a series of developmental processes and stress response (Schaller et al., 2018); Tsubulata_005706 closest homolog, *AtSDD1*, is a negative regulator of stomata density (Yoo et al., 2011). The detection of a Tsubulata_005706 peptide exclusively in the L-morph suggests that it's a key player for repression of filament elongation in the L-morph. This is supported by other characterized subtilase family members in floral development; *AcSBT1.8* negatively regulates cell proliferation in the petals of pineapple, and a wheat homolog of *SSD1* influences spikelet development (Zheng et al., 2016), and may play roles in male fertility in *Maize* (Hou et al., 2023) and tomato (Sheoran et al., 2009). Because subtilases do not solely suppress elongation, but rather finely regulate pathways related to elongation, Tsubulata_005706 may be a prime candidate for regulation of elongation in the L-morph, given that elongation still occurs in the L-morph, just to a lesser extent.

Five of the 13 proteins identified only in S-morph filaments are part of gene families that are involved in cell proliferation or elongation. In conjunction with the phosphoproteomic results (see below), the proteomic results

suggest that both cell proliferation and elongation are important for filament dimorphisms.

Phosphoproteomic analysis identifies phosphorylation events associated with PIK-related kinases

Since only a handful of differentially expressed proteins were identified, and *TsSPH1* encodes a putative signaling peptide that may mediate filament elongation via phosphosignaling cascades, we quantified protein phosphorylation as a complementary analysis to our proteomic analysis. We identified 5535 phosphopeptides from 2023 unique proteins; 46 of which were differentially phosphorylated ($p < 0.01$, $FC \leq 0.05$ or $FC \geq 1.5$), four were L-morph-specific or not detected in the S-morph, and 22 were S-morph-specific or not detected in the L-morph (Appendix S1: Figure S3C, D; Appendix S3).

Using our proteomic data set, which was generated using the "flowthrough" of our phosphopeptides experiment, we were able to confirm that two L-morph-specific and 16 S-morph-specific phosphorylation events were not artifacts of differential protein expression (Figure 3). The remaining morph-specific events could not be confirmed or rejected given the absence of unmodified protein data in the flowthrough data set, and we thus cannot conclude whether those particular phosphorylation differences are due to bona fide alterations in PTM levels rather than differential protein expression.

To explore the potential roles of these morph-specific phosphorylation events, we compared the phosphorylated residues to PhosPhAT (accessed 9 November 2023), a database of reported phosphorylation events in *Arabidopsis* (Durek et al., 2010). Five of the 15 morph-specific sites were previously documented in *Arabidopsis* (Appendix S1: Table S3; Figures S3–S16).

All four of the S-morph-specific sites previously reported in *Arabidopsis* were identified in a phosphoproteomic study characterizing two serine/threonine protein kinases (ATM and ATR) in DNA damage response and repair (Roitinger et al., 2015). Given that DNA damage correlates with cell cycle progression, this may be related to a role of increased cell proliferation in the S-morph. Tsubulata_021548's closest homolog is AtEIN2, an ER membrane bound protein that mediates ethylene signaling. Phosphorylation of AtEIN2 results in its degradation and prevents ethylene response to varying degrees (Ju et al., 2012; Zhang et al., 2020). While the S-morph-specific site has not been characterized in *Arabidopsis* (Appendix S1: Figure S7), its presence may suggest that ethylene signaling is reduced in the S-morph, potentially to promote cell proliferation (Street et al., 2015), as phosphorylation of EIN2 by TOR prevents repression of elongation in *Arabidopsis* (Fu et al., 2021). Tsubulata_021205's closest homolog is At5PTase12 (Appendix S1: Figure S8); in *Arabidopsis* At5PTase12 is expressed during pollen tube elongation (Scholz et al., 2020) and its closest Maize homolog positively influences cell elongation (Avila et al., 2016), potentially supporting a role for Tsubulata_021205 in filament elongation. Tsubulata_027034's closest homolog is Rrp15p (Appendix S1: Figure S16); it's unknown what downstream effects phosphorylation of Rrp15p results in. However, phosphorylation Rrp15p has been recorded as associated pre-ribosomal particles during late stages of ribosome assembly (Kruiswijk et al., 1978), potentially suggesting increased ribosome production in the S-morph. Tsubulata_014924, a homolog of RNA splicing factor RSp31, has two S-specific events occurring in its "RS" domain (Appendix S1: Figure S17); phosphorylation within this domain causes stabilization of the C- terminal end of the protein and ensures nuclear localization (Ghosh and Adams, 2011; Xiang et al., 2013), suggesting increased stability of the protein in the S-morph relative to that of the L-morph.

The sole L-morph-specific phosphorylation event occurs in Tsubulata_004956, a homolog of *CYP63*. CYP63 is a "multidomain" cyclophilin, likely involved in RNA splicing (Romano et al., 2004). The shared phosphorylation site (Appendix S1: Figure S4) was identified in a phosphoproteomic study targeting interaction partners of TOR, a PIK-related kinase (Van Leene et al., 2019).

Phosphorylation of Rrp15p, a homolog of Tsubulata_014924 (S-morph-specific), was also observed in the same TOR data set as CYP63. Given that TOR-related-pathways directly regulate cell cycle, endoreduplication, and growth (Shu et al., 2018; McCready et al., 2020; Burkart and Brandizzi, 2021), the presence of these TOR-correlated phosphorylation events may indicate hypothetical role for the genes in regulation of cell cycle and cell size in the filament. This is further supported by the phosphorylation of Tsubulata_021548, whose homolog EIN2 is directly phosphorylated by TOR (Fu et al., 2021).

Finally, the phosphorylation event identified in Tsubulata_002967 has not been documented in *Arabidopsis*. Tsubulata_002967 is a homolog of hypothetical serine/threonine protein kinase AT3G48187 and ATM1/AT3G48190 (Appendix S1: Figure S12). It contains an S-morph-specific phosphorylation event at T391. This phosphosite is not conserved in *Arabidopsis*; rather, in AT3G48187 there is an asparagine at the homologous position. ATM1 is a serine/threonine PIK-related kinase that promotes meiosis and fertility, mitosis, double-stranded break prevention, and crossing-over (Bosotti et al., 2000; Waterworth et al., 2016; Kurzbauer et al., 2021). This phosphorylation event may be of interest to future studies, as the presence of the residue and its subsequent phosphorylation may indicate neofunctionalization of the gene. A role for ATM1 in regulating filament elongation is further supported by the aforementioned S-morph phosphorylation events, which were all previously observed in a phosphoproteomic study exploring ATM1's role in DNA repair (Roitinger et al., 2015).

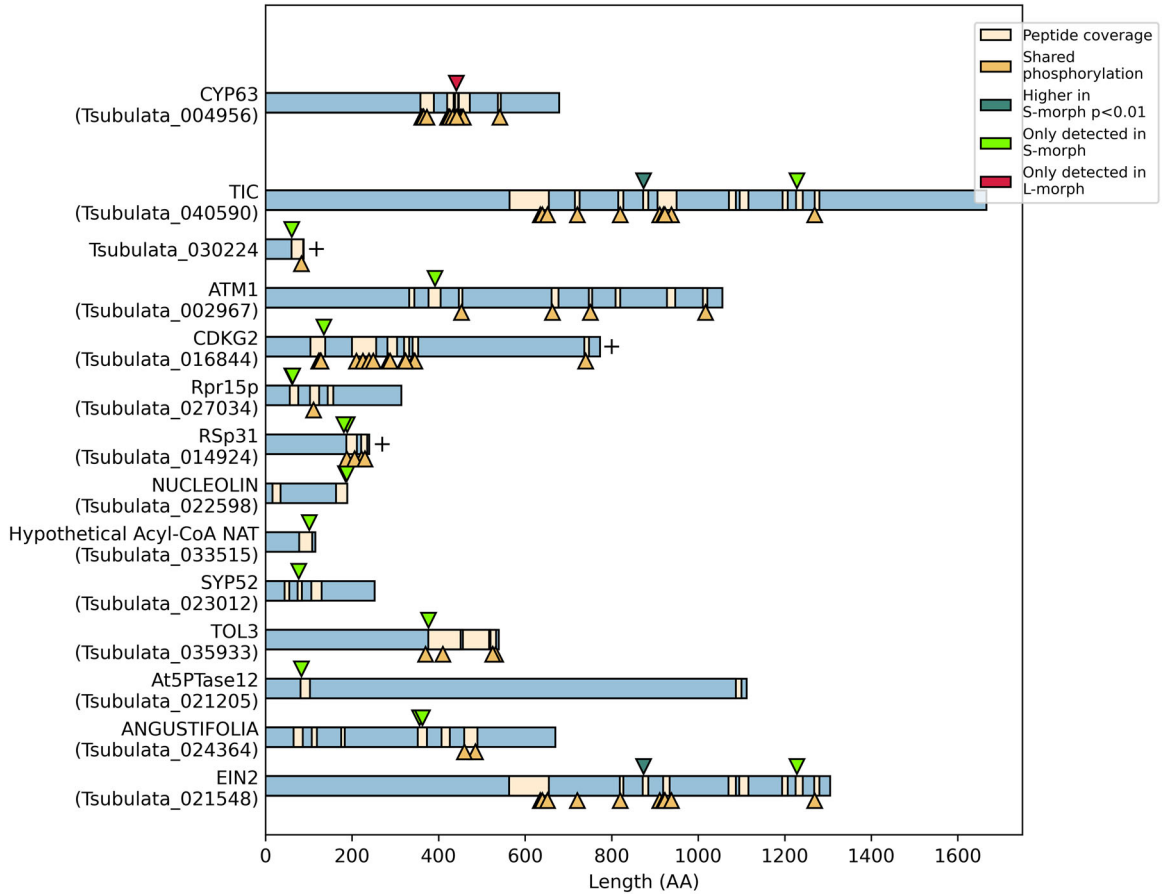

FIGURE 3 Visualization of morph-specific phosphorylation events. The L-morph-specific event resides at the top of the graph; the remainder are S-morph-specific. Arrowheads indicate phosphorylation site (see key for color code). Plus signs denote peptides that were not in the flowthrough data set, but the phosphorylation data set contained additional peptides whose site(s) were not differentially phosphorylated.

Gene co-expression analysis and clustering identifies clusters containing PIK-related kinases and *TsSPH1*

To identify pathways and support our proteomic and phosphoproteomic analyses, we generated the first co-expression network for the developing filaments of the S-morph of *T. subulata*. We found that 9168 genes are co-expressed in the developing filaments of the S-morph; 32 weighted gene co-expression network analysis (WGNCA) modules were identified within this co-expression network (Appendix S4; Appendix S1: Table S1). Among the proteins identified with MS, 3884 from the flowthrough samples and 1548 from the phosphoenriched samples mapped to the co-expression network (Appendix S1: Figure S18). WGNCA identified 32 modules. Phosphopeptides mapped to 11 of these modules and proteins to 18 modules (Appendix S1: Table S4).

TsSPH1 has 19 first neighbors, is part of the turquoise WGNCA-generated module that contained the highest portion of differentially expressed proteins and differentially phosphorylated peptides, and part of five clusters within said module (Appendix S1: Table S1). One cluster was of unique interest due to its higher clique score (0.838) and the higher portion of genes with MS-identified protein or phosphoprotein (hereafter "cluster 0.838"; Figure 4). Cluster 0.838 contains 165 genes, ~59% of which had representative peptides identified in the phosphoenriched data set and ~67% of which had representative peptides identified in the flowthrough data set. Among those with representative phosphopeptides, 11 are significantly differentially phosphorylated and two are S-morph-specific. Among those with representative unmodified peptides, 11 exhibit higher expression in the S-morph and two are L-morph-specific.

According to GO terms associated with the *Turnera* genes' closest *A. thaliana* homologs, terms related to reproductive structure development, binding, and membrane-bound organelles are among the most enriched (Appendix S2), supporting that the module is related to filament elongation.

Cluster 0.838 contains Tsubulata_009220, a homolog of TOR, and Tsubulata_015692, a homolog of RAPTOR—a binding partner of TOR (Burkart and Brandizzi, 2021). Together, TOR and RAPTOR regulate a series of growth pathways, including the transition from vegetative to reproductive growth (McCready et al., 2020). This suggests

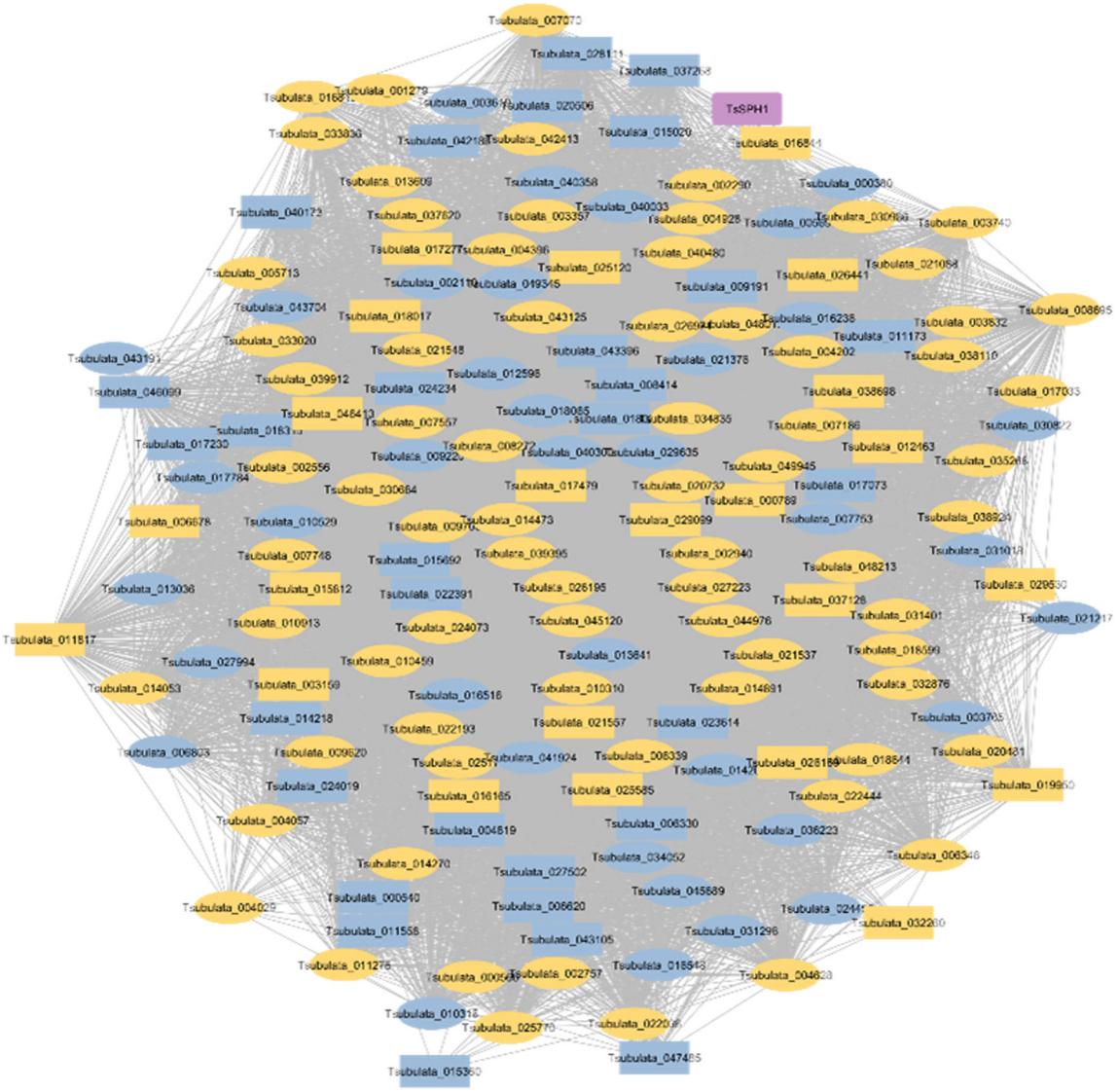

FIGURE 4 TsSPH1-containing cluster 0.838. Yellow = present in phosphoproteomic data set, blue = absent in phosphoproteomic data set, purple = *S*-gene; oval = present in flowthrough data set, rectangle = absence in flowthrough data set. Clique score 0.838.

that proteins associated with TOR-RAPTOR pathways may be important for establishing filament dimorphisms.

STRING analysis identifies a series of genes related to cell cycle progression and cell size regulation

To help identify TOR-RAPTOR-related pathways in cluster 0.838, we compiled a list of cluster 0.838's *Turnera* genes' closest *Arabidopsis* homologs and used STRING to generate an empirically supported *Arabidopsis* network (Figure 5). STRING network analysis of the *Turnera* homologs identified a strongly supported network containing TOR-RAPTOR and other known interactors (Figure 5; Table 1), supporting a potential role for TOR-RAPTOR in establishing filament dimorphisms. Empirical evidence from *Lilium* suggests herkogamy can be achieved via manipulation of downstream components of TOR-RAPTOR-related pathways. Exogenous expression of *Lilium longiflorum LS6K1*, a hypothetical $p70^{s6k}$ that acts downstream of TOR-mediated pathways, in *Arabidopsis* produced herkogamous flowers via decreased filament elongation due to decreased cell elongation (Tzeng et al., 2009) and is consistent with our hypothesis that TOR-related pathways may be involved in filament dimorphisms.

To further understand the role of TOR-RAPTOR-related pathways, we searched for TOR-related proteins in the STRING network generated for cluster 0.838 (Table 1). Tsubulata_025175 (CCT) was initially of interest; a single phosphopeptide was detected at similar levels in both the S- and L-morph phosphoproteomic data sets, but an unmodified second peptide was detected only in the L-morph (normalized average abundance of 94195.78),

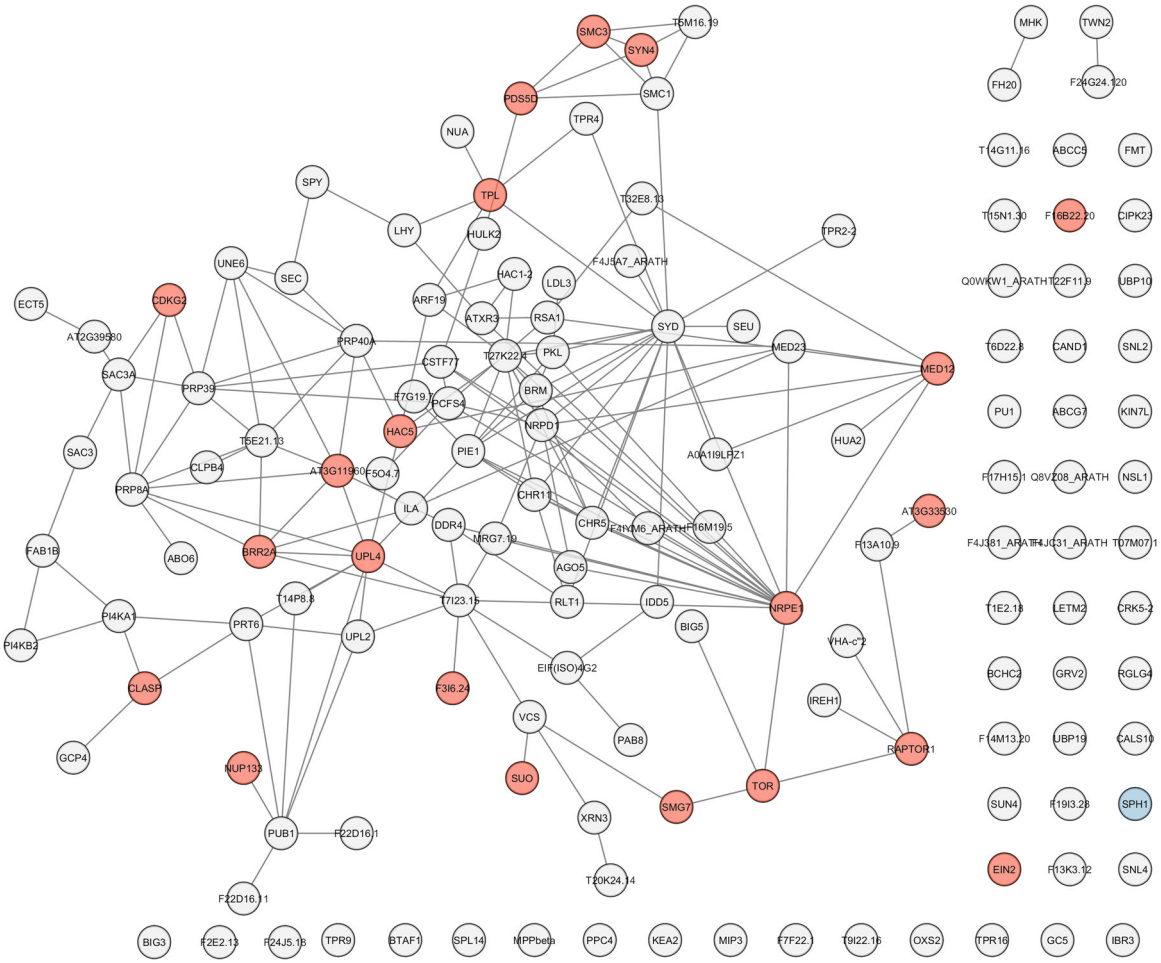

FIGURE 5 STRING-generated *Arabidopsis* homolog network of cluster 0.838. This network identified an empirically supported subnetwork containing TOR and RAPTOR. Genes referenced in the present study are highlighted in red; SPH1 is highlighted in blue.

suggesting that unmodified Tsubulata_025175 is not present in the S-morph or is expressed at levels below our limit of detection in the S-morph. CCT was not previously identified as differentially expressed in the stamen of *T. subulata* or *T. joelii* (Henning et al., 2020), suggesting that differential expression at the protein level occurs post-transcriptionally.

Tsubulata_025175 is a homolog of *CRYPTIC PRECOCIOUS* (*CCT/CRP/MED12*), a mediator of RNA synthesis. CCT is part of the Cyclin Dependent kinase module (CKM) that regulates transcription in conjunction with GCT/MED13, CDK8, and CycC via mediating interactions between transcription factors and transcriptional machinery, specifically NRPB1, the largest subunit of RNA polymerase (Agrawal et al., 2021). In mammals and yeast, MED12 and MED13 are negative regulators of the CKM complex, preventing the core of the complex from interacting with the transcriptional machinery (Agrawal et al., 2021); loss of function of MED12 in yeast results in early entry into the mitotic cycle (Banyai et al., 2014), and phosphorylation of MED13 in yeast results in the degradation of MED13, resulting in increased cell division (Stieg et al., 2018).

In plants, CCT and GCT regulate the transition from vegetative growth to flowering (Gillmor et al., 2014). CCT is a negative regulator of *FLC* and a positive regulator of several flower-related genes, including *FT* and *SOC1* (Imura et al., 2012; Gillmor et al., 2014). Beyond the transition from the vegetative stage to flowering, several of the CCT-regulated genes influence floral morphogenesis (Deng et al., 2011). For example, alteration of the expression of *SOC1* in *Viola* determines whether a flower is destined to be chasmogamous (CH) or cleistogamous (CL) (Li et al., 2022). CL flowers lack visible filaments, while their CH counterparts have visible filaments (Li et al., 2022). Supporting that, alteration of CCT-regulated pathways can result in herkogamous flowers. In *Arabidopsis*, loss of function *cct* mutants show a stamen to petal phenotype, suggesting a major role in the regulation of stamen morphogenesis (Imura et al., 2012). This previous work, in suggesting that the protein may bear some influence on the L-morph's morphology, supported our interest in CCT.

Phosphorylation of CCT/MED12 has not been explored in any system. As phosphorylation of CCT's synergistic homolog GCT results in degradation in yeast, phosphorylation of CCT

TABLE 1 Differential (SvL) phosphorylation or expression events in cluster 0.838.

Turnera subulata	Phosphorylation			Flowthrough			Closest *A. thaliana* homolog	
Transcript ID	Y/N	FC	*p*	FC	*p*	STG	ID	TAIR description (paraphrased)
Tsubulata_002290	Y	N/A	N/A	2.891	0.0922	N	AT2G41900	AtOXS2 specifically entered the nuclear under salt stress. The specific nuclear localization of AtOXS2 could play a role in salt tolerance at the molecular level.
Tsubulata_002940	Y	1.651	0.0107	2.225	0.0376	Y	AT3G12980	Encodes an enzyme with histone acetyltransferase activity that can use both H3 and H4 histones as substrates.
	Y	1.65	0.0204					
Tsubulata_004202	Y	1.559	0.0467	1.094	N/A	Y	AT1G24300	GYF domain-containing protein.
Tsubulata_007186	Y	1.74	0.0213	1.138	N/A	N	AT4G00630	Encodes a K(+)/H(+) antiporter that modulates monovalent cation and pH homeostasis in plant chloroplasts or plastids.
		3.3	0.0083					
Tsubulata_007753	N	N/A	N/A	0.001	L-morph	Y	AT3G33530	Transducin family protein/WD-40 repeat family protein.
Tsubulata_010459	Y	1.55	0.0562	1.808	0.0011	Y	AT3G11960	Cleavage and polyadenylation specificity factor (CPSF) A subunit protein.
Tsubulata_014473	Y	1.873	0.0437	1.030	N/A	Y	AT1G15750	Protein with several WD40 repeats at the C-terminus and predicted protein-protein interaction domains at the N-terminus. Together with TP, it's thought to be involved in transcriptional repression of root-promoting genes in the top half of the embryo. Interacts with IAA12 through the EAR domain of IAA12 and the CTLH domain of TPL.
Tsubulata_016236	N	N/A	N/A	2.364	0.0304	N	AT2G25320	TRAF-like family protein.
Tsubulata_021548	Y	1000	S-morph	0.992	N/A	N	AT5G03280	EIN2. Involved in ethylene signal transduction. Acts downstream of CTR1. Positively regulates ORE1 and negatively regulates mir164A,B,C to regulate leaf senescence. Mutations in ein2 block ethylene stimulation of flavanol synthesis.
		3.204	0.0054					
Tsubulata_025175	Y	N/A	N/A	0.001	L-morph	Y	AT4G00450	*Arabidopsis* homolog of the transcriptional regulator MED12, is dynamically expressed during embryogenesis. Regulates developmental timing and radial pattern formation. A knockout mutant of this gene showed late-flowering phenotype.
Tsubulata_026195	Y	1.891	0.0391	1.58	0.0167	N	AT2G35050	Raf-like kinase required for stomatal vapor pressure difference response.
Tsubulata_026971	Y	2.711	0.0352	1.128	N/A	Y	AT5G02880	Encodes a ubiquitin-protein ligase containing a HECT domain.
Tsubulata_037620	Y	1.708	0.0006	0.891	N/A	Y	AT2G20190	Encodes a microtubule-associated protein that is involved in both cell division and cell expansion. It likely promotes microtubule stability.
Tsubulata_038924	Y	1.843	0.0484	1.528	0.0575	Y	AT1G24300	GYF domain-containing protein.
Tsubulata_042413	Y	1.776	0.0267	1.143	N/A	Y	AT3G48050	Encodes a large protein with N-terminal bromo-adjacent homology and transcription elongation factor S-II domains and two C-terminal GW repeats. SOU is a component of the miRNA pathway.
Tsubulata_048013	Y	N/A	N/A	2.627	0.0310	Y	AT2G05120	Nucleoporin, Nup133/Nup155-like protein.
Tsubulata_049945	Y	0.448	0.0248	0.964	N/A	Y	AT1G80810	One of 5 PO76/PDS5 cohesion cofactor orthologs of *Arabidopsis*.
		2.353	0.0028					

Note: Phosphorylation Y/N = Peptide was identified in the phosphorylation data set, Y = identified, N = not identified, gray indicates phosphorylation in global TOR phosphorylation analysis (Van Leene et al., 2019). FC: phosphorylated peptides without a fold change (FC) are denoted by N/A. Peptides identified in only one of the two morphs are denoted by the morph they are specific to. Colors correspond to morph: green = more abundant in the S-morph, shades of orange = more abundant in the L-morph. STG Y/N = if *A. thaliana* homolog is part of the STRING-identified TOR associated network.

in *T. subulata* may result in its degradation in both morphs to promote cell division. Observation of unmodified CCT solely in the L-morph is consistent with a model in which overexpression of CCT in the L-morph results in increased repression of CKM in the L-morph compared to the S-morph.

To explore the possibility of differential CKM regulation between the morphs due to overabundance of CCT in the L-morph, we searched for associated proteins in cluster 0.838. Although GCT and CycC homologs were not identified, we did identify a CDKG2 homolog, Tsubulata_016844, which is phosphorylated only in the S-morph and is not present in the flowthrough of either morph. The presence of phosphorylated CDKG2 may suggest that the kinase is active solely in the S-morph.

In *A. thaliana*, AtCDKG2/AT1G67580 promotes endoreduplication and cell growth/expansion while repressing cell division (Jiang et al., 2022). CYCLIN DEPENT-KINASE B1;1 (AtCDKB1;1) negatively regulates AtCDKG2 activity by phosphorylation at Ser-728 (Jiang et al., 2022). The closest *T. subulata* homolog of AtCDKB1;1 is Tsubulata_025697, did not associate with the turquoise module and thus its expression does not correlate with filament elongation. CDKB1;1 showed higher expression in the L-morph (FC = 0.587), but the fold change was above what is considered differentially expressed in this analysis. Ser-728 was not identified as phosphorylated in our data set (Appendix S1: Figure S10), suggesting that TsCDKB1;1 is not actively repressing TsCDKG2 activity in the S-morph. Interestingly, Tsubulata_037153, a type-A cyclin, is also found in the same module as CDKB1;1 and shows higher phosphorylation in the L-morph, albeit again below what is considered a significant fold change (FC = 0.501). Type-A cyclin, AtCYCA2;3, interacts with AtCDKB1;1 to repress endoreduplication (Boudolf et al., 2009). It does not appear that *T. subulata* has a "close" homolog to AtCYCA2;3. AtCYCA3;4 is the closest *A. thaliana* homolog of Tsubulata_037153, which appears to interact with AtCDKB1;1, but it is unknown what this interaction induces (Leene et al., 2007).

To date, there isn't any evidence of interaction between CDKG2 and CTT, so the co-occurrence of these phosphorylation events may be arbitrary. However, the yeast homolog of CDKB1;1 (PHO85) interacts with SRB8, the yeast homolog of CCT (Breitkreutz et al., 2010; Oughtred et al., 2021). The function of this interaction is currently unknown (due to lethality of double knockouts; Tong et al., 2004).

Several genes related to flowering were upregulated in the S-morph—for example, CPSF30 Tsubulata_010459 (FC = 1.808), FY Tsubulata_021823 (FC = 25.011), and CTR9 Tsubulata_028004 (FC = 1.54). Several flowering-related genes were also differentially phosphorylated: REF6 Tsubulata_030824 (FC = 2.325) and SUMO Tsubulata_001914 (FC = 1.671).

A large number of genes related to flowering time and morphology were neither differentially expressed nor differentially phosphorylated (i.e., FT homolog, Tsubulata_043588, FC = 0.999; three homologs of HRLP, Tsubulata_002743, FC = 1.159, Tsubulata_024670, FC = 0.682; Tsubulata_006803, FC = 0.723; BRR2 homolog Tsubulata_045120, FC = 1.282), suggesting that pathways related to general flowering and floral morphology are still functional in both morphs. This was expected, as the L-morph has visible filaments and thus lends confidence to the data set as a whole.

It should be noted that although co-expression analyses provide insights into large data sets and their biological relevance while simultaneously alleviating the tremendous amount of time required to understand the data set, some data will be lost. The hypotheses formed here must be supported with empirical data, and genes not discussed in the present study may be of biological relevance but arbitrarily neglected here because of the large nature of the data set. We identified several differentially expressed genes related to flowering that were not part of cluster 0.838 such as AGL5 Tsubulata_004879 (FC = 1.577) and SWP73A Tsubulata_003189 (FC = 3.337); thus, genes outside of cluster 0.838 should not be dismissed as unimportant for herkogamy. Further exploration into genes outside of cluster 0.838 is required to fully grasp the presence of reciprocal herkogamy in *Turnera* and will be the subject of future studies.

Expression patterns of closely related *SPH* paralogs suggest that neofunctionalization of *TsSPH1* is reliant on changes in subcellular localization

Previously, it was hypothesized that altered *TsSPH1* expression resulted in neofunctionalization, not alteration of the sequence itself, given that *SPH1*'s closest paralogs are not expressed in the flower yet form an orthologous group with *SPH1* (Henning et al., 2023). To test this hypothesis, we examined expression patterns of *TsSPH1*'s closest *Populus* and *Manihot* homologs (Appendix S1: Figure S19; Tables S5 and S6). Phylogenetic analysis revealed that more distant *Turnera* homologs formed a subclade with the *Populus*, *Salix*, and *Manihot* homologs. The sole *Turnera* homolog that is expressed in the bud (Tsubulata_012609) is also expressed in the filament but is not part of cluster 0.838 (Appendix S4). Of the five *SPH*s expressed in *Populus*, three are male-bud-specific. The other two are expressed in both male and female buds, but at higher levels in the female bud. Taking into consideration the other Malpighiales homologs' expression patterns, the data suggests that the last common ancestor of these homologs was expressed in the stamen and/or filament.

We further explored hypothetical neofunctionalization of *TsSPH1* via alteration of expression by computationally predicting subcellular localization. While computational programs have only an 87.88% success rate at predicting subcellular localization (Sahu et al., 2020), they can be an important tool for forming hypotheses for future lab-work,

especially in non-model organisms. Our computational analysis predicts that *TsSPH1* and two-thirds of the *Populus* male *SPH*s localize to the Golgi, while *TsSPH1*'s closest paralogs localize to the extracellular region. These results suggest that subcellular localization is important for *TsSPH1*'s role in establishing filament dimorphisms. Alternatively, as computationally predicted subcellular localization relies on predicted protein properties in addition to motifs and sequence homology (Sahu et al., 2020), neofunctionalization of TsSPH1 may depend on protein chemistry that is not easily observed via sequence alignments. Investigation into the biochemical properties of TsSPH1 and its closest *Turnera* paralogs is required to understand how, or if, *TsSPH1*'s function has changed from the ancestral gene's function.

DISCUSSION

A key trait of all distylous species is reciprocal herkogamy. While the molecular basis of style length dimorphisms has been explored thoroughly in *Primula* (Huu et al., 2016, 2021; Liu et al., 2024) and *Turnera* (Henning et al., 2020; Matzke et al., 2020, 2021), the molecular basis of anther height dimorphisms, beyond their associated *S*-genes' hypothetical roles, remains a mystery in most distylous species. Here, we explored the molecular basis of filament dimorphisms in *T. subulata* using a multi-omic approach. We propose the first model for how stamen height dimorphisms are established in the L-morph of any distylous genera. Additionally, we have identified several proteins and pathways of interest for future empirical work.

Upstream regulation of endoreduplication may be essential for establishing filament dimorphisms

Filament length dimorphisms, which result in anther height dimorphisms in *Turnera*, are established via increased cell elongation, as determined by microscopy, which may be a result of endoreduplication, a process by which cell size is increased via duplication of the genome (Shu et al., 2018). Endoreduplication is commonly used by plants as a means to rapidly grow (Shu et al., 2018), potentially explaining the rapid filament growth observed in the S-morph in comparison to the "slow" and steady pistil growth observed in the L-morph.

We propose a model by which filament elongation is repressed in the L-morph via degradation of CDKG2 (Tsubulata_016844) by CDKB1;1 (Tsubulata_025697; Figure 6). CDKG2 induces the entrance of the cell into the endocycle (Jiang et al., 2022), likely via the interactions with CYCLA (Tourdot et al., 2023). Given that CDKG2 peptides and phosphorylated peptides were identified only in the S-morph samples, and CDKB1;1 showed higher expression in the L-morph (FC = 0.587), it is possible that endoreduplication is repressed in the L-morph via degradation of CDKG2 by CDKB1;1. S-morph-specific phosphorylation of CDKG2 and higher levels of phosphorylation of CYCLA (Tsubulata_051490, FC = 1.814, $p = 0.0034$) would suggest that the complex is active solely in the S-morph.

S-morph-specific phosphorylation of TsATM1 supports this model, in that AtATM1 responds to double-stranded breaks (DSB) in DNA during the endoreduplication cycle (Adachi et al., 2011; Kurzbauer et al., 2021). In response to DSB, AtATM1 activates AtSOG1, a transcription factor that

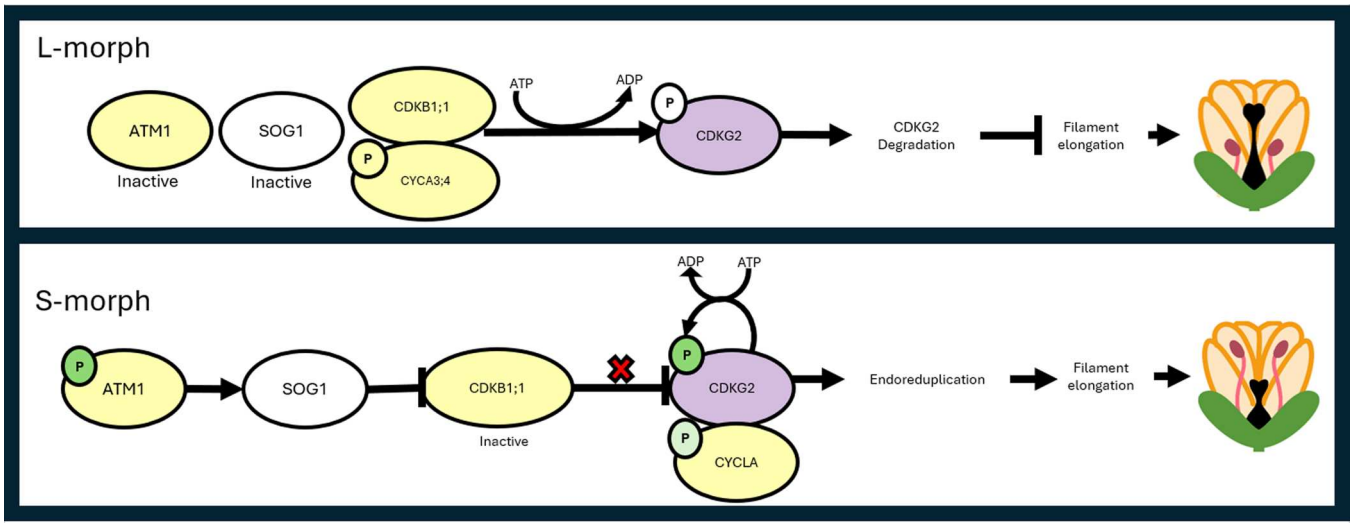

FIGURE 6 Proposed model for filament elongation in the S-morph. In the S-morph, active ATM1 repressed CDKB1;1 activity, resulting in CDKG2 inducing the endoreduplication cycle. In the L-morph, CDDKB1;1 phosphorylates CDKG2, resulting in its degradation, preventing the cell from entering the endoreduplication cycle. Dark green indicates phosphorylation only in the S-morph; light green indicates higher phosphorylation in the S-morph; purple indicates non-phosphorylated peptide not identified. Yellow indicates not significantly differentially expressed or phosphorylated. White protein indicates identified by RNAseq but not mass spectrometry. White phosphorylation represents a site not identified in the data set but referenced in the present study.

represses the expression of CDKB1;1 (Weimer et al., 2016). *TsSOG1* mRNA (Tsubulata_030168) was identified in our analysis, but peptides were not, potentially due to the limitations of MS. The absence of the phosphorylated residue of TsATM1 in its closest *Arabidopsis* homolog (Appendix S1: Figure S12) suggests that TsATM1 has undergone some degree of neofunctionalization in *Turnera*, potentially related to inducing endoreduplication in the filament in response to TsSPH1 perception.

First neighbors of *TsSPH1* also support the hypothetical importance of the endocycle in filament length dimorphism. *SYN4* (Tsubulata_040033) and *PDS5B* (Tsubulata_033020) are involved in DSB repair in *Arabidopsis* (da Costa-Nunes et al., 2014; Pradillo et al., 2015). *SMC3* (Tsubulata_041924) maintains sister chromatid cohesion during meiosis (Bolaños-Villegas, 2021) and during endoreduplication in *Drosophila* to maintain genome stability (Stormo and Fox, 2019). Additionally, due to the overlap of proteins involved in both cell cycle and endoreduplication, the differential expression and phosphorylation of proteins discussed throughout this study that are related to or regulated by the cell cycle, likely support the hypothetical importance of endoreduplication in filament elongation. The large overlap of these processes convolutes further hypothesis formation. Empirical investigation into the roles of SPH1, CDKG2, and ATM1 is required to better understand the depths of this data set.

The role of TsSPH1 in filament elongation remains a mystery

TsSPH1 is the *S*-gene required for filament elongation in the S-morph as determined by short-filament S-morph mutants (Shore et al., 2019), yet TsSPH1's role in filament elongation remains unclear. Our network analysis revealed that several of *TsSPH1*'s first neighbors were related to the cell cycle and DNA damage repair (Appendix S4) and that *TsSPH1* clusters with the genes discussed in Figure 6. This may be indicative of a putative role in mediating phosphorylation of cell-cycle-related genes to induce endoreduplication, as potentially supported by the one characterized member of the *SPH* family, PrsS, that triggers programmed cell death (PCD; Wilkins et al., 2015). Genome instability is associated with both endoreduplication and PCD (Fox and Duronio, 2013), and PrsS perception by its receptor actives a caspase-3-like protein (Bosch and Franklin-Tong, 2007). Caspase-3-like proteins regulate both apoptosis and cell cycle progression (Hashimoto et al., 2011), potentially supporting a role for TsSPH1 in triggering endoreduplication. Further exploration of TsSPH1's interaction partners is required to better understand its role in filament elongation.

Our analysis of close *TsSPH1* homologs suggests that the ancestral expression patterns of *TsSPH1* have been maintained, as close homologs are filament- or male-bud-expressed. That said, predicted subcellular localization of TsSPH1 suggests that its localization has changed from its ancestral state; while its closest homologs are predicted to localize to the extracellular space, TsSPH1 is predicted to localize to the Golgi. The predicted extracellular localization suggests that the ancestral gene was involved in extracellular signaling, whereas TsSPH1 may be involved in intercellular/transcriptional signaling.

Commonalities with the *Primula* system—manipulation of MADS-box genes results in herkogamy

Anther height dimorphisms rely on increased cell elongation, as observed in some species of distylous *Primula* (Huu et al., 2020). While several proteins related to cell proliferation were differentially expressed, due to the convoluted nature of endoreduplication and mitosis, this result requires empirical investigation, though the data set may suggest that cell cycle progression is reduced in the L-morph.

It appears that anther height dimorphisms in *Primula* and *Turnera* are established via manipulation of MADS-box genes. In *Primula*, stamen height dimorphisms are established by the *S*-gene GLO^T, a MADS-box gene. That said, it is unknown which pathways are directly affected by the presence/absence of GLO^T or how stamen height is determined in the L-morph in *Primula*.

Our data suggest that in the L-morph of *Turnera*, increased CCT expression represses expression of genes related to flower morphogenesis, including MADS-box gene *AGL5*, and to cell cycle. Empirical exploration of the role of CCT in the L-morph is required to truly understand what these changes in expression levels result in.

While there are apparently similarities with the *Primula* system (i.e., the hypothetical use of MADS-box genes to achieve anther height dimorphisms), the discrepancy proposed is that MADS-box and other flowering genes establish the phenotype observed in the L-morph of *Turnera*, not the S-morph.

CONCLUSIONS

Little was known regarding filament dimorphisms in distylous *Turnera* aside from the necessity of *TsSPH1*. To explore the molecular basis of filament dimorphisms, we employed a multi-omic approach in hopes of identifying TsSPH1 regulated pathways. Our analysis strongly suggests that endoreduplication is essential for filament elongation in the S-morph. Our analysis has identified several proteins that may be of interest for future empirical work and has identified commonalities between PrsS from *Papaver* and TsSPH1 from *Turnera*.

AUTHOR CONTRIBUTIONS

Conceptualization: P.M.H. and M.R.S. Methodology: P.M.H. and B.B.M. Software: P.M.H. and B.B.M. Formal analyses: P.M.H. Resources: P.M.H. and M.R.S. Data

curation: P.M.H. Visualization: P.M.H. Original draft preparation: P.M.H. Review and editing: all authors. All authors have read and agreed to the published version of the manuscript.

ACKNOWLEDGMENTS

We thank the National Science Foundation for funding this work (no. 2208975), J. Shore for providing his input on the manuscript, and the reviewers whose input greatly strengthened the manuscript.

CONFLICT OF INTERESTS STATEMENT

The authors declare no conflict of interest.

DATA AVAILABILITY STATEMENT

RNAseq files have been uploaded to GenBank (Bioproject no. PRJNA1054211; https://www.ncbi.nlm.nih.gov/bioproject/PRJNA1054211). Raw MS/MS files have been uploaded to ProteomeXchange (PXD049414; https://proteomecentral.proteomexchange.org/cgi/GetDataset?ID=PXD049414). Co-expression network and clusters have been uploaded to NDex (network set 8b31d902-857d-11ee-8a13-005056ae23aa; https://www.ndexbio.org/#/networkset/8b31d902-857d-11ee-8a13-005056ae23aa?accesskey=59e425466a551d6260939e2d243d7fdb7cbf4ae2f04a505f8985e28fd005e620).

ORCID

Paige M. Henning http://orcid.org/0000-0002-4145-4733

REFERENCES

Adachi, S., K. Minamisawa, Y. Okushima, S. Inagaki, K. Yoshiyama, Y. Kondou, E. Kaminuma, et al. 2011. Programmed induction of endoreduplication by DNA double-strand breaks in *Arabidopsis*. *Proceedings of the National Academy of Sciences of the United States of America* 108: 10004–10009.

Agrawal, R., F. Jiří, and J. K. Thakur. 2021. The kinase module of the Mediator complex: an important signalling processor for the development and survival of plants. *Journal of Experimental Botany* 72: 224–240.

Altschul, S., T. L. Madden, A. A. Schaffer, J. Zhang, Z. Zhang, W. Miller, and D. J. Lipman. 1997. Gapped BLAST and PSI-BLAST: a new generation of protein database search programs. *Nucleic Acids Research* 25: 3389–3402.

Avila, L. M., D. Cerrudo, C. Swanton, and L. Lukens. 2016. *Brevis plant1*, a putative inositol polyphosphate 5-phosphatase, is required for internode elongation in maize. *Journal of Experimental Botany* 67: 1577–1588.

Banyai, G., M. D. Lopez, Z. Szilagyi, and C. M. Gustafsson. 2014. Mediator Can Regulate Mitotic Entry and Direct Periodic Transcription in Fission Yeast. *Molecular and Cellular Biology* 34: 4008–4018.

Barrett, S. C. H. 2019. 'A most complex marriage arrangement': recent advances on heterostyly and unresolved questions. *New Phytologist* 224: 1051–1067.

Benton, M. J., P. Wilf, and H. Sauquet. 2022. The Angiosperm Terrestrial Revolution and the origins of modern biodiversity. *New Phytologist* 233: 2017–2035.

Bolaños-Villegas, P. 2021. The Role of Structural Maintenance of Chromosomes Complexes in Meiosis and Genome Maintenance: Translating Biomedical and Model Plant Research Into Crop Breeding Opportunities. *Frontiers in Plant Science* 12: 659558.

Bosch, M., and V. E. Franklin-Tong. 2007. Temporal and spatial activation of caspase-like enzymes induced by self-incompatibility in Papaver pollen. *Proceedings of the National Academy of Sciences* 104: 18327–18332.

Bosotti, R., A. Isacchi, and E. L. L. Sonnhammer. 2000. FAT: a novel domain in PIK-related kinases. *Trends in Biochemical Sciences* 25: 225–227.

Boudolf, V., T. Lammens, J. Boruc, J. Van Leene, H. Van Den Daele, S. Maes, G. Van Isterdael, et al. 2009. CDKB1;1 Forms a Functional Complex with CYCA2;3 to Suppress Endocycle Onset. *Plant Physiology* 150: 1482–1493.

Breitkreutz, A., H. Choi, J. R. Sharom, L. Boucher, V. Neduva, B. Larsen, Z. -Y. Lin, et al. 2010. A global protein kinase and phosphatase interaction network in yeast. *Science* 328: 1043–1046.

Burkart, G. M., and F. Brandizzi. 2021. A Tour of TOR Complex Signaling in Plants. *Trends in Biochemical Sciences* 46: 417–428.

Cardoso, J. C. F., M. L. Viana, R. Matias, M. T. Furtado, A. P. D. S. Caetano, H. Consolaro, and V. L. G. D. Brito. 2018. Towards a unified terminology for angiosperm reproductive systems. *Acta Botanica Brasilica* 32: 329–348.

Cocker, J. M., J. Wright, J. Li, D. Swarbreck, S. Dyer, M. Caccamo, and P. M. Gilmartin. 2018. Primula vulgaris (primrose) genome assembly, annotation and gene expression, with comparative genomics on the heterostyly supergene. *Scientific Reports* 8: 17942.

da Costa-Nunes, J. A., C. Capitão, J. Kozak, P. Costa-Nunes, G. M. Ducasa, O. Pontes, and K. J. Angelis. 2014. The AtRAD21.1 and AtRAD21.3 *Arabidopsis* cohesins play a synergistic role in somatic DNA double strand break damage repair. *BMC Plant Biology* 14: 353.

Danecek, P., J. K. Bonfield, J. Liddle, J. Marshall, V. Ohan, M. O. Pollard, A. Whitwham, et al. 2021. Twelve years of SAMtools and BCFtools. *GigaScience* 10: giab008.

Darwin, C. 1877. The different forms of flowers on plants of the same species. D. Appleton and Co., New York.

de Graaf, B. H. J., S. Vatovec, J. A. Juárez-Díaz, L. Chai, K. Kooblall, K. A. Wilkins, H. Zou, et al. 2012. The Papaver Self-Incompatibility Pollen S-Determinant, PrpS, Functions in *Arabidopsis thaliana*. *Current Biology* 22: 154–159.

Deng, W., H. Ying, C. A. Helliwell, J. M. Taylor, W. J. Peacock, and E. S. Dennis. 2011. FLOWERING LOCUS C (FLC) regulates development pathways throughout the life cycle of *Arabidopsis*. *Proceedings of the National Academy of Sciences* 108: 6680–6685.

Doncheva, N. T., J. H. Morris, J. Gorodkin, and L. J. Jensen. 2019. Cytoscape StringApp: Network Analysis and Visualization of Proteomics Data. *Journal of Proteome Research* 18: 623–632.

Durek, P., R. Schmidt, J. L. Heazlewood, A. Jones, D. MacLean, A. Nagel, B. Kersten, and W. X. Schulze. 2010. PhosPhAt: the *Arabidopsis thaliana* phosphorylation site database. An update. *Nucleic Acids Research* 38: D828–D834.

Edgar, R. C. 2004. MUSCLE: multiple sequence alignment with high accuracy and high throughput. *Nucleic Acids Research* 32: 1792–1797.

Fawcett, J. A., R. Takeshima, S. Kikuchi, E. Yazaki, T. Katsube-Tanaka, Y. Dong, M. Li, et al. 2023. Genome sequencing reveals the genetic architecture of heterostyly and domestication history of common buckwheat. *Nature Plants* 9: 1236–1251.

Fox, D. T., and R. J. Duronio. 2013. Endoreplication and polyploidy: insights into development and disease. *Development* 140: 3–12.

Franklin-Tong, V. E. 2008. Self-Incompatibility in Flowering Plants. Springer Berlin Heidelberg, Berlin, Heidelberg.

Franklin-Tong, V. E., J. P. Ride, and F. C. H. Franklin. 1995. Recombinant stigmatic self-incompatibility (S-) protein elicits a Ca2+ transient in pollen of Papaver rhoeas. *The Plant Journal* 8: 299–307.

Fu, L., Y. Liu, G. Qin, P. Wu, H. Zi, Z. Xu, X. Zhao, et al. 2021. The TOR–EIN2 axis mediates nuclear signalling to modulate plant growth. *Nature* 591: 288–292.

Ghosh, G., and J. A. Adams. 2011. Phosphorylation Mechanism and Structure of Serine-Arginine Protein Kinases. *The FEBS Journal* 278: 587–597.

Gillmor, C. S., C. O. Silva-Ortega, M. R. Willmann, M. Buendía-Monreal, and R. S. Poethig. 2014. The *Arabidopsis* Mediator CDK8 module genes CCT (MED12) and GCT (MED13) are global regulators of developmental phase transitions. *Development (Cambridge, England)* 141: 4580–4589.

Goodstein, D. M., S. Shu, R. Howson, R. Neupane, R. D. Hayes, J. Fazo, T. Mitros, et al. 2012. Phytozome: a comparative platform for green plant genomics. *Nucleic Acids Research* 40: D1178–D1186.

Gutiérrez-Valencia, J., M. Fracassetti, E. L. Berdan, I. Bunikis, L. Soler, J. Dainat, V. E. Kutschera, et al. 2022. Genomic analyses of the Linum distyly supergene reveal convergent evolution at the molecular level. *Current Biology* 32: 4360-4371.e6.

Hashimoto, T., U. Kikkawa, and S. Kamada. 2011. Contribution of Caspase (s) to the Cell Cycle Regulation at Mitotic Phase. *PLoS One* 6: e18449.

Heazlewood, J. L., P. Durek, J. Hummel, J. Selbig, W. Weckwerth, D. Walther, and W. X. Schulze. 2008. PhosPhAt: a database of phosphorylation sites in *Arabidopsis thaliana* and a plant-specific phosphorylation site predictor. *Nucleic Acids Research* 36: D1015-D1021.

Henning, P. M., E. H. Roalson, W. Mir, A. G. McCubbin, and J. S. Shore. 2023. Annotation of the Turnera subulata (Passifloraceae) Draft Genome Reveals the S-Locus Evolved after the Divergence of Turneroideae from Passifloroideae in a Stepwise Manner. *Plants* 12: 286.

Henning, P. M., J. S. Shore, and A. G. McCubbin. 2022. The S-Gene YUC6 pleiotropically determines male mating type and pollen size in *Heterostylous turnera* (Passifloraceae): A novel neofunctionalization of the YUCCA gene family. *Plants* 11: 2640.

Henning, P. M., J. S. Shore, and A. G. McCubbin. 2020. Transcriptome and network analyses of heterostyly in *Turnera subulata* provide mechanistic insights: Are S-Loci a red-light for pistil elongation? *Plants* 9: 713.

Hou, Q., L. Wang, Y. Qi, T. Yan, F. Zhang, W. Zhao, and X. Wan. 2023. A systematic analysis of the subtilase gene family and expression and subcellular localization investigation of anther-specific members in maize. *Plant Physiology and Biochemistry* 203: 108041.

Huu, C. N., C. Kappel, B. Keller, A. Sicard, Y. Takebayashi, H. Breuninger, M. D. Nowak, et al. 2016. Presence versus absence of CYP734A50 underlies the style-length dimorphism in primroses. *eLife* 5: e17956.

Huu, C. N., B. Keller, E. Conti, C. Kappel, and M. Lenhard. 2020. Supergene evolution via stepwise duplications and neofunctionalization of a floral-organ identity gene. *Proceedings of the National Academy of Sciences* 117: 23148–23157.

Huu, C. N., S. Plaschil, A. Himmelbach, C. Kappel, and M. Lenhard. 2021. Female self-incompatibility type in heterostylous Primula is determined by the brassinosteroid-inactivating cytochrome P450 CYP734A50. *Current Biology* 32: 671–676.

Imura, Y., Y. Kobayashi, S. Yamamoto, M. Furutani, M. Tasaka, M. Abe, and T. Araki. 2012. CRYPTIC PRECOCIOUS/MED12 is a novel flowering regulator with multiple target steps in *Arabidopsis*. *Plant and Cell Physiology* 53: 287–303.

Jiang, S., J. Wei, N. Li, Z. Wang, Y. Zhang, R. Xu, L. Zhou, et al. 2022. The UBP14-CDKB1;1-CDKG2 cascade controls endoreduplication and cell growth in *Arabidopsis*. *The Plant Cell* 34: 1308–1325.

Jiang, X.-F., X.-F. Zhu, and Q.-J. Li. 2018. Variation in the degree of reciprocal herkogamy affects the degree of legitimate pollination in a distylous species. *AoB Plants* 10: ply022.

Jones, D. T., W. R. Taylor, and J. M. Thornton. 1992. The rapid generation of mutation data matrices from protein sequences. *Computer Applications in the Biosciences* 8: 275–282.

Ju, C., G. M. Yoon, J. M. Shemansky, D. Y. Lin, Z. I. Ying, J. Chang, W. M. Garrett, et al. 2012. CTR1 phosphorylates the central regulator EIN2 to control ethylene hormone signaling from the ER membrane to the nucleus in *Arabidopsis*. *Proceedings of the National Academy of Sciences* 109: 19486–19491.

Karron, J. D., D. A. Christopher, and W. R. Semski. 2021. Pollen transport: Illuminating a key mechanism of disassortative pollination. *Current Biology* 31: R893–R895.

Kruiswijk, T., J. T. de Hey, and R. J. Planta. 1978. Modification of yeast ribosomal proteins. *Phosphorylation. Biochemical Journal* 175: 213–219.

Kurzbauer, M.-T., M. P. Janisiw, L. F. Paulin, I. Prusén Mota, K. Tomanov, O. Krsicka, A. von Haeseler, et al. 2021. ATM controls meiotic DNA double-strand break formation and recombination and affects synaptonemal complex organization in plants. *The Plant Cell* 33: 1633–1656.

Leene, J. V., H. Stals, D. Eeckhout, G. Persiau, E. V. D. Slijke, G. V. Isterdael, A. D. Clercq, et al. 2007. A tandem affinity purification-based technology platform to study the cell cycle interactome in *Arabidopsis thaliana*. *Molecular & Cellular Proteomics* 6: 1226–1238.

Li, Q., K. Li, Z. Zhang, J. Li, B. Wang, Z. Zhang, Y. Zhu, et al. 2022. Transcriptomic comparison sheds new light on regulatory networks for dimorphic flower development in response to photoperiod in *Viola prionantha*. *BMC Plant Biology* 22: 336.

Liu, Y., W. Si, S. Fu, J. Wang, T. Cheng, Q. Zhang, and H. Pan. 2024. *PfPIN5* promotes style elongation by regulating cell length in *Primula forbesii* French. *Annals of Botany* 133: 473–482.

de Lucas, M., and S. Prat. 2014. PIFs get BRright: PHYTOCHROME INTERACTING FACTORs as integrators of light and hormonal signals. *New Phytologist* 202: 1126–1141.

Luo, Y., and A. Widmer. 2013. Herkogamy and its effects on mating patterns in *Arabidopsis thaliana*. *PLoS One* 8: e57902.

Matzke, C. M., H. J. Hamam, P. M. Henning, K. Dougherty, J. S. Shore, M. M. Neff, and A. G. McCubbin. 2021. Pistil mating type and morphology are mediated by the brassinosteroid inactivating activity of the S-locus gene BAHD in heterostylous Turnera species. *International Journal of Molecular Sciences* 22: 10603.

Matzke, C. M., J. S. Shore, M. M. Neff, and A. G. McCubbin. 2020. The Turnera Style S-Locus Gene TsBAHD Possesses Brassinosteroid-Inactivating Activity When Expressed in *Arabidopsis thaliana*. *Plants* 9: 1566.

McCready, K., V. Spencer, and M. Kim. 2020. The Importance of TOR Kinase in Plant Development. *Frontiers in Plant Science* 11: 16.

Naiki, A. 2012. Heterostyly and the possibility of its breakdown by polyploidization. *Plant Species Biology* 27: 3–29.

Oughtred, R., J. Rust, C. Chang, B. Breitkreutz, C. Stark, A. Willems, L. Boucher, et al. 2021. The BioGRID database: A comprehensive biomedical resource of curated protein, genetic, and chemical interactions. *Protein Science* 30: 187–200.

Perez-Riverol, Y., J. Bai, C. Bandla, D. García-Seisdedos, S. Hewapathirana, S. Kamatchinathan, D. J. Kundu, et al. 2022. The PRIDE database resources in 2022: a hub for mass spectrometry-based proteomics evidences. *Nucleic Acids Research* 50: D543–D552.

Pertea, M., D. Kim, G. M. Pertea, J. T. Leek, and S. L. Salzberg. 2016. Transcript-level expression analysis of RNA-seq experiments with HISAT, StringTie and Ballgown. *Nature Protocols* 11: 1650–1667.

Pillich, R. T., J. Chen, V. Rynkov, D. Welker, and D. Pratt. 2017. NDEx: A Community Resource for Sharing and Publishing of Biological Networks. *In* C. H. Wu, C. N. Arighi, and K. E. Ross [eds.], Protein Bioinformatics, Methods in Molecular Biology, 271–301. Springer New York, New York, NY.

Potente, G., R. L. Stubbs, N. Yousefi, W. Pirovano, P. Szövényi, and E. Conti. 2022. Comparative transcriptomics reveals commonalities and differences in the genetic underpinnings of a floral dimorphism. *Scientific Reports* 12: 20771.

Pradillo, M., A. Knoll, C. Oliver, J. Varas, E. Corredor, H. Puchta, and J. L. Santos. 2015. Involvement of the Cohesin Cofactor PDS5 (SPO76) During Meiosis and DNA Repair in *Arabidopsis thaliana*. *Frontiers in Plant Science* 6: 1034.

R Core Team. 2023. R: A Language and Environment for Statistical Computing.

Roitinger, E., M. Hofer, T. Köcher, P. Pichler, M. Novatchkova, J. Yang, P. Schlögelhofer, and K. Mechtler. 2015. Quantitative Phosphoproteomics of the Ataxia Telangiectasia-Mutated (ATM) and Ataxia Telangiectasia-Mutated and Rad3-related (ATR) Dependent DNA Damage Response in *Arabidopsis thaliana*. *Molecular & Cellular Proteomics* 14: 556–571.

Romano, P. G. N., P. Horton, and J. E. Gray. 2004. The Arabidopsis Cyclophilin Gene Family. *Plant Physiology* 134: 1268–1282.

RStudio Team. 2020. RStudio: Integrated Development for R.

Rueden, C. T., J. Schindelin, M. C. Hiner, B. E. DeZonia, A. E. Walter, E. T. Arena, and K. W. Eliceiri. 2017. ImageJ2: ImageJ for the next generation of scientific image data. *BMC Bioinformatics* 18: 529.

Sahu, S. S., C. D. Loaiza, and R. Kaundal. 2020. Plant-mSubP: a computational framework for the prediction of single- and multi-target protein subcellular localization using integrated machine-learning approaches. *AoB Plants* 12: plz068.

Sauquet, H., S. Ramírez-Barahona, and S. Magallón. 2022. What is the age of flowering plants? *Journal of Experimental Botany* 73: 3840–3853.

Schaffer, A. A., L. Aravind, T. L. Madden, S. Shavirin, J. L. Spouge, Y. I. Wolf, E. V. Koonin, and S. F. Altschul. 2001. Improving the accuracy of PSI-BLAST protein database searches with composition-based statistics and other refinements. *Nucleic Acids Research* 29: 2994–3005.

Schaller, A., A. Stintzi, S. Rivas, I. Serrano, N. V. Chichkova, A. B. Vartapetian, D. Martínez, et al. 2018. From structure to function – a family portrait of plant subtilases. *New Phytologist* 218: 901–915.

Scholz, P., J. Anstatt, H. E. Krawczyk, and T. Ischebeck. 2020. Signalling Pinpointed to the Tip: The Complex Regulatory Network That Allows Pollen Tube Growth. *Plants* 9: 1098.

Shannon, P. 2003. Cytoscape: A Software Environment for Integrated Models of Biomolecular Interaction Networks. *Genome Research* 13: 2498–2504.

Sheoran, I. S., A. R. S. Ross, D. J. H. Olson, and V. K. Sawhney. 2009. Differential expression of proteins in the wild type and 7B-1 male-sterile mutant anthers of tomato *(Solanum lycopersicum)*: A proteomic analysis. *Journal of Proteomics* 71: 624–636.

Shore, J. S., H. J. Hamam, P. D. J. Chafe, J. D. J. Labonne, P. M. Henning, and A. G. McCubbin. 2019. The long and short of the *S* -locus in *Turnera* (Passifloraceae). *New Phytologist* 224: 1316–1329.

Shu, Z., S. Row, and W.-M. Deng. 2018. Endoreplication: The Good, the Bad, and the Ugly. *Trends in Cell Biology* 28: 465–474.

Stieg, D. C., S. D. Willis, V. Ganesan, K. L. Ong, J. Scuorzo, M. Song, J. Grose, et al. 2018. A complex molecular switch directs stress-induced cyclin C nuclear release through SCFGrr1-mediated degradation of Med13. *Molecular Biology of the Cell* 29: 363–375.

Stormo, B. M., and D. T. Fox. 2019. Interphase cohesin regulation ensures mitotic fidelity after genome reduplication. *Molecular Biology of the Cell* 30: 219–227.

Street, I. H., S. Aman, Y. Zubo, A. Ramzan, X. Wang, S. N. Shakeel, J. J. Kieber, and G. E. Schaller. 2015. Ethylene Inhibits Cell Proliferation of the *Arabidopsis* Root Meristem. *Plant Physiology* 169: 338–350.

Tamura, K., and M. Nei. 1993. Estimation of the number of nucleotide substitutions in the control region of mitochondrial DNA in humans and chimpanzees. *Molecular Biology and Evolution* 10: 512–526.

Tamura, K., G. Stecher, and S. Kumar. 2021. MEGA11: Molecular Evolutionary Genetics Analysis Version 11 F. *Molecular Biology and Evolution* 38: 3022–3027.

Tong, A. H. Y., G. Lesage, G. D. Bader, H. Ding, H. Xu, X. Xin, J. Young, et al. 2004. Global mapping of the yeast genetic interaction network. *Science* 303: 808–813.

Tourdot, E., J.-P. Mauxion, N. Gonzalez, and C. Chevalier. 2023. Endoreduplication in plant organogenesis: a means to boost fruit growth. *Journal of Experimental Botany* 74: 6269–6284.

Tzeng, T.-Y., L.-R. Kong, C.-H. Chen, C.-C. Shaw, and C.-H. Yang. 2009. Overexpression of the Lily p70s6k Gene in *Arabidopsis* Affects Elongation of Flower Organs and Indicates TOR-Dependent Regulation of AP3, PI and SUP Translation. *Plant and Cell Physiology* 50: 1695–1709.

Van Leene, J., C. Han, A. Gadeyne, D. Eeckhout, C. Matthijs, B. Cannoot, N. De Winne, et al. 2019. Capturing the phosphorylation and protein interaction landscape of the plant TOR kinase. *Nature Plants* 5: 316–327.

Walker, E. A., J. P. Ride, S. Kurup, V. E. Franklin-Tong, M. J. Lawrence, and F. C. H. Franklin. 1996. Molecular analysis of two functional homologues of the S 3 allele of the Papaver rhoeas self-incompatibility gene isolated from different populations. *Plant Molecular Biology* 30: 983–994.

Waterworth, W. M., S. Footitt, C. M. Bray, W. E. Finch-Savage, and C. E. West. 2016. DNA damage checkpoint kinase ATM regulates germination and maintains genome stability in seeds. *Proceedings of the National Academy of Sciences* 113: 9647–9652.

Weimer, A. K., S. Biedermann, H. Harashima, F. Roodbarkelari, N. Takahashi, J. Foreman, Y. Guan, et al. 2016. The plant-specific CDKB1-CYCB1 complex mediates homologous recombination repair in *Arabidopsis*. *The EMBO Journal* 35: 2068–2086.

Wilkins, K. A., M. Bosch, T. Haque, N. Teng, N. S. Poulter, and V. E. Franklin-Tong. 2015. Self-Incompatibility-Induced Programmed Cell Death in Field Poppy Pollen Involves Dramatic Acidification of the Incompatible Pollen Tube Cytosol. *Plant Physiology* 167: 766–779.

Wilson, M. C., A. M. Mutka, A. W. Hummel, J. Berry, R. D. Chauhan, A. Vijayaraghavan, N. J. Taylor, et al. 2017. Gene expression atlas for the food security crop cassava. *New Phytologist* 213: 1632–1641.

Xiang, S., V. Gapsys, H.-Y. Kim, S. Bessonov, H.-H. Hsiao, S. Möhlmann, V. Klaukien, et al. 2013. Phosphorylation Drives a Dynamic Switch in Serine/Arginine-Rich Proteins. *Structure* 21: 2162–2174.

Yang, J., H. Xue, Z. Li, Y. Zhang, T. Shi, X. He, S. C. H. Barrett, et al. 2023. Haplotype-resolved genome assembly provides insights into the evolution of *S*-locus supergene in distylous *Nymphoides indica*. *New Phytologist* 240: 2058-2071.

Yoo, C. Y., P. M. Hasegawa, and M. V. Mickelbart. 2011. Regulation of stomatal density by the GTL1 transcription factor for improving water use efficiency. *Plant Signaling & Behavior* 6: 1069–1071.

Zhang, J., Y. Chen, J. Lu, Y. Zhang, and C.-K. Wen. 2020. Uncertainty of EIN2Ser645/Ser924 Inactivation by CTR1-Mediated Phosphorylation Reveals the Complexity of Ethylene Signaling. *Plant Communications* 1: 100046.

Zhao, Z., Y. Zhang, M. Shi, Z. Liu, Y. Xu, Z. Luo, S. Yuan, et al. 2023. Genomic evidence supports the genetic convergence of a supergene controlling the distylous floral syndrome. *New Phytologist* 237: 601–614.

Zheng, X., H. Liu, H. Ji, Y. Wang, B. Dong, Y. Qiao, M. Liu, and X. Li. 2016. The Wheat GT Factor TaGT2L1D Negatively Regulates Drought Tolerance and Plant Development. *Scientific Reports* 6: 27042.

SUPPORTING INFORMATION

Additional supporting information can be found online in the Supporting Information section at the end of this article.

Appendix S1. Supplemental figures, methods, and tables.

Figure S1. Additional photos of the flowers of *T. subulate*.

Figure S2. Proteome discoverer pipeline.

Figure S3. MS identified peptides.

Figure S4. ClustalW alignment Tsubulata_004956 and homologs.

Figure S5. ClustalW alignment Tsubulata_024364 and homologs.

Figure S6. ClustalW alignment Tsubulata_012162 and homologs.

Figure S7. ClustalW alignment Tsubulata_021548 and homologs.

Figure S8. ClustalW alignment Tsubulata_035933 and homologs.

Figure S9. ClustalW alignment Tsubulata_021205 and homologs.

Figure S10. ClustalW alignment Tsubulata_016844 and homologs.

Figure S11. ClustalW alignment Tsubulata_022598 and homologs.

Figure S12. ClustalW alignment Tsubulata_002967 and homologs.

Figure S13. ClustalW alignment Tsubulata_030224 and homologs.

Figure S14. ClustalW alignment Tsubulata_040590 and homologs.

Figure S15. ClustalW alignment Tsubulata_033515 and homologs.

Figure S16. ClustalW alignment Tsubulata_027034 and homologs.

Figure S17. ClustalW alignment Tsubulata_014924 and homologs.

Figure S18. Overlap of -omic data.

Figure S19. Phylogenetic cladogram of *SPH1*'s closest homologs.

Methods S1. Protein purification.

Methods S2. Co-expression commands.

Table S1. Ndex IDs.

Table S2. Morph-specific proteins.

Table S3. Documented *Arabidopsis* phosphorylation events.

Table S4. Proteins and phosphopeptides associated with WGNCA modules.

Table S5. Close homologs of *TsSPH1*.

Table S6. Genomes used for phylogenetic analysis.

Appendix S2. MS identified peptides.

Appendix S3. MS identified phospho-peptides.

Appendix S4. Co-expression network and GO terms.

How to cite this article: Henning, P. M., B. B. Minkoff, and M. R. Sussman. 2024. Phosphoproteomic analysis of distylous *Turnera subulata* identifies pathways related to endoreduplication that correlate with reciprocal herkogamy. *American Journal of Botany* 111(12): e16438. https://doi.org/10.1002/ajb2.16438